© 2017. Published by The Company of Biologists Ltd | Journal of Experimental Biology (2017) 220, 266-277 doi:10.1242/jeb.149211

RESEARCH ARTICLE

Retinal specialization through spatially varying cell densities and opsin coexpression in cichlid fish

Brian E. Dalton[1], Fanny de Busserolles[2], N. Justin Marshall[2] and Karen L. Carleton[1,*]

ABSTRACT

The distinct behaviours of animals and the varied habitats in which animals live place different requirements on their visual systems. A trade-off exists between resolution and sensitivity, with these properties varying across the retina. Spectral sensitivity, which affects both achromatic and chromatic (colour) vision, also varies across the retina, though the function of this inhomogeneity is less clear. We previously demonstrated spatially varying spectral sensitivity of double cones in the cichlid fish *Metriaclima zebra* owing to coexpression of different opsins. Here, we map the distributions of ganglion cells and cone cells and quantify opsin coexpression in single cones to show these also vary across the retina. We identify an area centralis with peak acuity and infrequent coexpression, which may be suited for tasks such as foraging and detecting male signals. The peripheral retina has reduced ganglion cell densities and increased opsin coexpression. Modeling of cichlid visual tasks indicates that coexpression might hinder colour discrimination of foraging targets and some fish colours. But, coexpression might improve contrast detection of dark objects against bright backgrounds, which might be useful for detecting predators or zooplankton. This suggests a trade-off between acuity and colour discrimination in the central retina versus lower resolution but more sensitive contrast detection in the peripheral retina. Significant variation in the pattern of coexpression among individuals, however, raises interesting questions about the selective forces at work.

KEY WORDS: Vision, Retina, Spectral sensitivity, Visual acuity

INTRODUCTION

For animals in a broad range of environments, vision mediates diverse behaviours, including navigation, foraging, territorial conflict and mate choice. Different visual tasks may place different demands on the visual system. The aquatic environment provides perhaps the greatest diversity of habitat types, certainly in terms of light level or spectral content differences. Within this watery realm, there are also a dazzling variety of feeding, mating and territorial behaviours, many of which rely on colour vision to gather information. For example, avoiding a distant predator may require detecting its silhouette against the background, while choosing a mate might involve evaluating the patches of colour a suitor displays. The mate's gaze likely fixates on these colour patches, stabilizing their image on the central region of the retina. Meanwhile, if a predator approaches from above, its silhouette will move swiftly across the ventral retina. Thus, different types of behaviour and visual tasks may require different regions of the retina to specialize for different functions. How these regions of the retina are specialized for different tasks is not well understood in most animals, despite a number of careful studies and reviews (Hughes, 1985; Temple, 2011). The cichlids from the African rift lake system are a diverse and fascinating group to study with a well-characterized genetic and phylogenetic history. Here, using both genetic and anatomical tools, we examine how the visual tasks and visual environment of one of the best known cichlid species, *Metriaclima zebra* (Boulenger, 1899), have shaped its unique retinal design.

The acuity of many vertebrates is spatially inhomogeneous across the retina. In animals that move and fixate their eyes to examine specific objects, acuity often reaches its peak in a fovea or an area centralis, where retinal ganglion cell densities are highest (Land and Nilsson, 2001). Alternatively, there may be a visual streak of high acuity, especially for animals that interact with an extended horizon or water surface (Hughes, 1985; Land and Nilsson, 2001). In this way, the demands of the outside world are in some way mirrored in retinal design, both among photoreceptors and in other cells further down the neural pathway, such as ganglion cells. Ganglion cells ultimately transmit visual signals to the brain down the optic nerve, and therefore set the upper limit of spatial resolution. For a given eye size there is a trade-off required between resolution and absolute sensitivity (Land and Nilsson, 2001). While one retinal area, such as a fovea, may be adapted for high resolution, other regions, such as a ventral-viewing periphery, may show morphological or molecular adaptations for enhanced sensitivity.

Spectral sensitivity also varies across the retina in many animals, though the functional significance of this is generally unknown (Temple, 2011). In several cases, intra-retinal variation in spectral sensitivities (and ganglion cell densities) has been shown to correlate with variation in the light environment (Baden et al., 2013; Briscoe et al., 2003; Owens et al., 2012; Temple et al., 2010; Dalton et al., 2014). The backgrounds viewed by different retinal regions differ spectrally, both for aquatic and terrestrial organisms (Dalton et al., 2014; Endler, 1993; Munz and McFarland, 1977). A simple example is the difference between the sky and the land, a dorsal–ventral difference that has a profound effect on the retinal design of most terrestrial animals (Baden et al., 2013).

Spectral sensitivity of a photoreceptor is primarily determined by its visual pigment, composed of an opsin protein bound to a chromophore. We previously showed that in the African cichlid fish *M. zebra*, spectral sensitivity of double cones is tuned across the retina by differential coexpression of two distinct pairs of opsins (Dalton et al., 2014). *Metriaclima zebra* double cones, which are paired cone cells common among vertebrates, consist of two spectrally distinct members, a medium wavelength sensitive (M) member and a long wavelength sensitive (L) member. M-cones

[1]Department of Biology, University of Maryland, College Park, MD 20742, USA.
[2]Queensland Brain Institute, University of Queensland, Brisbane 4072, Australia.

*Author for correspondence (kcarleto@umd.edu)

K.L.C., 0000-0001-6306-5643

Received 9 September 2016; Accepted 25 October 2016

Journal of Experimental Biology

Journal of Experimental Biology (2017) 220, 266-277 doi:10.1242/jeb.149211

express *RH2B* opsin (λ_{max}=484 nm) and L-cones express *RH2Aalpha* (528 nm). M-cones can also coexpress *RH2Abeta* (519 nm) predominantly in the nasal retina, while L-cones can coexpress *LWS* (567 nm) in the ventral retina.

Here, we map expression of *SWS1* and *SWS2B* opsins (368 and 423 nm; Parry et al., 2005) in short wavelength sensitive (S) single cones of this species to complete the picture of cone sensitivity across the retina. We also map cone cell and ganglion cell densities so that patterns of acuity and absolute sensitivity can be related to spectral sensitivity. Finally, using visual models, we examine possible visual function across the retina in terms of the distributions of cone cells, ganglion cells and opsin coexpression. We show that the retina of *M. zebra* has an area centralis with higher ganglion and photoreceptor densities and low coexpression in all three cone classes. Modelling suggests that this region may be specialized for high acuity vision with good colour discrimination. Higher opsin coexpression might enhance sensitivity in regions of reduced ganglion cell density and spatial acuity. However, there is considerable variation among individuals in how much coexpression occurs. This raises the possibility that coexpression is more complex, possibly being either non-functional in the current evolutionary landscape or under relaxed selection (Wertheim et al., 2015).

MATERIALS AND METHODS

All fish were reared in the same light environment, which, compared with natural *M. zebra* habitat, is rich in long wavelength light and has no ultraviolet light (Dalton et al., 2015). Rearing and handling of fish were carried out in accordance with an approved IACUC protocol (University of Maryland R15-54). Retinas were obtained from laboratory-reared descendants of *M. zebra* collected from Mazinzi Reef in Lake Malawi.

Cell densities

Preparation of retinal wholemounts

The eyes of four individuals of *M. zebra* were enucleated, the cornea and lens dissected out and the eye cups fixed in 4% paraformaldehyde in 0.1 mol l^{-1} phosphate buffer (PBS) overnight at 4°C. Retinal wholemounts were then dissected according to standard protocols (Stone et al., 1981; Coimbra et al., 2006; Ullmann et al., 2012). The orientation of the retina was kept by referring to the position of the optic nerve head, which is directed ventrally but slightly rotated (15–30 deg) toward the nasal area, and the falciform process, which ends ventrally. Remnants of the retinal pigment epithelium, which could not be removed mechanically during dissection, were bleached overnight in a solution of 3% hydrogen peroxide in PBS (Coimbra et al., 2009).

To analyze photoreceptor cells, retinas were directly flatmounted with the photoreceptor layer facing up, and placed on a microscope slide in a solution of 80% glycerol in PBS. For the analysis of ganglion cells, the retinas were wholemounted, ganglion cell layer facing up, on a gelatinized slide and left to dry overnight in formalin vapour to improved fixation and cell differentiation (Coimbra et al., 2006, 2012; Ullmann et al., 2012). Wholemounts were then stained in 0.1% Cresyl Violet following the protocol of Coimbra et al. (2006) and finally mounted with Entellan New (Merck). Possible shrinkage during staining was considered negligible and if present confined to the retina margin, as the retinal wholemount was attached to the slide during the entire staining process (Coimbra et al., 2006).

Stereological analyses and topographic map construction

Following the protocols described in de Busserolles et al. (2014a, 2014b), topographic distribution of single cones, double cones, total cones and ganglion cells were assessed using the optical fractionator technique (West, 1991) modified by Coimbra et al. (2009, 2012) for use in retinal whole mounts. Briefly, for each whole mount, the outline of the retina was digitized using a ×5 objective (numerical aperture 0.16) mounted on a compound microscope (Zeiss Imager.Z2) equipped with a motorized stage (MAC 6000 System, Microbrightfield, USA), a digital colour camera (Microbrightfield) and a computer running StereoInvestigator software (Microbrightfield). Cells were randomly and systematically counted using a ×40 air objective (numerical aperture 0.75) for cones, and a ×63 oil objective (numerical aperture 1.40) for ganglion cells.

The counting frame and grid size were carefully chosen to maintain the highest level of sampling and achieve an acceptable Schaeffer coefficient of error (CE). The CE is a measure of the accuracy of the total number of cell estimates and is considered acceptable below 0.1 (Slomianka and West, 2005; Glaser and Wilson, 1998). Because the four individuals analyzed were of similar sizes, the same stereological parameters, that is a counting frame of 100×100 µm and a grid size of 650×650 µm, were used for all individuals to allow for comparison. For ganglion cells analysis, sub-sampling using the same counting frame but a smaller grid (325×325 µm) was also performed in the area of highest density to verify the peak density estimate. The total number of cells was estimated by multiplying the sum of total neurons counted by the area of the sampling fraction (i.e. ratio between the counting frame and the sampling grid).

Single cones and double cones were counted separately and simultaneously using two different markers to generate data for single cones alone, double cones alone and the two cell types combined (total cones). Ganglion cells were arranged in a single layer and were easily identified from other cell types (displaced amacrine cells and glial cells) using cytological criteria alone (Collin and Collin, 1988; Hughes, 1975). As a result, amacrine cells and glial cells were excluded from the analysis and only ganglion cells were counted in this study.

Topographic maps were constructed using the statistical program R v3.1.1 (R Foundation for Statistical Computing, Vienna, Austria) with the results exported from Stereo Investigator software according to Garza-Gisholt et al. (2014). For each map we used the Gaussian Kernel Smoother from the Spatstat package (Baddeley and Turner, 2005) and adjusted the sigma value to the grid size (i.e. 650).

Spatial resolving power estimation

The upper limit of spatial resolving power (SRP) in cycles deg^{-1} was estimated for three individuals of *M. zebra* using the peak density of ganglion cells, as described by Collin and Pettigrew (1989):

$$SRP = (PDG/\alpha)/2, \quad (1)$$

where PDG is the peak linear density of ganglion cells in cells mm^{-1} and α is the angle subtending 1 mm on the retina, calculated using the following formula:

$$\alpha = \arctan(1/f). \quad (2)$$

Here f is the lens focal length in teleost fishes, and taken to be 2.55 times the radius of the lens (Matthiessen, 1882). A visual element that has a width x and is y distance away, will subtend an angle θ:

$$\theta = \sin^{-1}(x/y). \quad (3)$$

If θ is greater than 1/(2SRP) (because SRP depends on resolving two elements), then one element can be distinguished from its neighbour.

Journal of Experimental Biology (2017) 220, 266-277 doi:10.1242/jeb.149211

In situ hybridization

To map expression of opsins in single cones across the retina, we performed double labeling fluorescent *in situ* hybridization on whole retinas according to published methods (Allison et al., 2010; Barthel and Raymond, 2000; Dalton et al., 2014, 2015). After euthanizing fish, we removed retinas and fixed them in 4% paraformaldehyde overnight. To detect *SWS1* and *SWS2B* expression, we developed coding sequence probes labeled with digoxigenin (DIG) and fluorescein. Cross-hybridization is not expected between *SWS1* (NCBI accession AF191219.1) and *SWS2B* (AF317674.1) probes because the coding sequences of these genes have only 59% identity. Furthermore, *SWS2A* is not expressed by *M. zebra* (Hofmann et al., 2009; Smith et al., 2011). Probe signals were enzymatically enhanced with sequential tyramide signal amplification, using Alexa Fluor 594 and 488 dyes (Invitrogen) for the DIG and fluorescein probes, respectively. These dyes have distinct excitation spectra, preventing crosstalk. We used a Leica DM 5500B epifluorescence microscope with L5 and TX2 filter cubes to view retinas.

We examined opsin expression at approximately 30 locations distributed across each retina, with a higher density of sampling locations in specific areas of interest. In each sampling location, 50 single cones were examined for the presence of *SWS1* and *SWS2B* opsin transcripts, and the frequency of coexpression was calculated. We also performed this whole-retina examination on two retinas that we had probed in our previous studies of double cone opsin expression. We used one retina that was probed for *RH2Aalpha* and *LWS* (individual RI1 in table S3 from Dalton et al., 2015) and one probed for *RH2B* and *RH2Abeta* (individual 15 in fig. 3c from Dalton et al., 2014).

We produced a topographic map of each retina showing the frequency of coexpression. Maps were generated in RStudio (Version 0.99.489) using a thin plate smoothing function (Garza-Gisholt et al., 2014). Dorsal and nasal directions within topographic maps were determined using the optic nerve head for reference.

Colour discrimination and contrast detection

To examine the possible effects of opsin coexpression on visual function, we modelled colour discrimination and contrast detection by the *M. zebra* visual system in Lake Malawi light environments. We modelled the ability of the *M. zebra* trichromatic visual system to discriminate *M. zebra* colours from different viewing backgrounds and its ability to discriminate between foraging substrates. Colour discrimination was evaluated with a receptor-noise-limited model (Siddiqi et al., 2004; Vorobyev et al., 2001). As described below, there is one region of the retina with minimal coexpression, along with the four retinal quadrants, which each differ in coexpression combinations. We therefore modelled colour discrimination using pure (non coexpressing) pigments and compared that with coexpressing pigment combinations found in the four quadrants. Previous microspectrophotometry measurements of visual pigment mixtures in *M. zebra* double cones indicated coexpressing M-cones contained an average of 50% *RH2Abeta* mixed with *RH2B* and coexpressing L-cones contained an average of 30% *LWS* mixed with *RH2Aalpha* (Dalton et al., 2014). In addition, qPCR has suggested that gene ratios of *SWS2B*/*SWS1* can be as high as 50% in *M. zebra*. We therefore assume a 50/50 mixture of *SWS1* and *SWS2B* for coexpressing single cones.

In considering the visual tasks that are important to cichlids, we note that cichlids forage either by capturing zooplankton from the water column or by eating algae from rocks. During mating, males defend territories just above the rock substrate. As females swim above these territories, viewing males against the rocks, males will observe females above and ahead of them against the downwelling light. As females approach within a few meters, males will rise up to court females, with each sex then viewing the other against the background space light (Fig. 1). We therefore consider several scenarios: cichlid colours viewed against downwelling radiance at 30–60 deg; cichlid colours viewed against space light of 75–105 deg (with 90 deg being horizontal); and cichlid colours viewed against the rocks. We also consider whether cichlids can discriminate between different algal covered rocks, different colours with a cichlid colour pattern, or zooplankton from space light.

Environmental light spectra as well as reflectance measurements of *M. zebra* and Lake Malawi viewing backgrounds and foraging substrates were taken from Dalton et al. (2010, 2014), where each spectrum is an average of 10 measurements (Table S1). In the modelling, we used viewing conditions 3 m below the surface, a depth at which *M. zebra* are common. Radiance at different viewing angles (Table S1A) were previously quantified at several locations in the southeast arm of Lake Malawi, where *M. zebra* are common, including Thumbi West Island (Dalton et al., 2010), Mazinzi Reef (Dalton et al., 2014) and Otter Point (Sabbah et al., 2011). Four different rock substrates were used to represent viewing backgrounds as well as foraging substrates (Table S1B). We used a set of cichlid colours that includes male blues, yellows, blacks and white as well as female brown and green reflectance spectra taken for *M. zebra* (from Dalton et al., 2010; Table S1C).

We calculated the quantum catch of each cone class i, following Dalton et al. (2010), as:

$$Q_i = K_i \int_{300}^{700} R_i(\lambda)L(\lambda)S(\lambda)I(\lambda)\mathrm{d}\lambda, \quad (4)$$

where R_i is receptor sensitivity, L is lens transmittance, S is surface reflectance, I is the illuminant and K_i (Eqn 2) adjusts for von Kries colour constancy (Kelber et al., 2003):

$$K_i = \frac{1}{\int R_i(\lambda)L(\lambda)I(\lambda)\mathrm{d}\lambda}. \quad (5)$$

Receptor sensitivities are calculated using the equations of Govardovskii et al. (2000) based on *M. zebra* microspectrophotometry (Table S1D). Lens transmission was

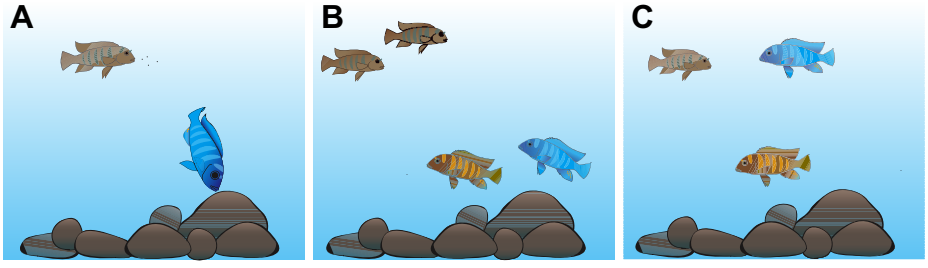

Fig. 1. Cichlid visual tasks. (A) Cichlids feed from the water column or eat aufwuchs/algae off rock substrates. (B) For mating, brown females initially view conspecific blue males against rocks, while males view females against the downwelling light. (C) If males decide to court, they will rise up into the water column, where males and females will view each other against the background space light. Drawings by D. Escobar-Camacho (modified from Escobar-Camacho and Carleton, 2015).

Journal of Experimental Biology

Journal of Experimental Biology (2017) 220, 266-277 doi:10.1242/jeb.149211

measured in the field (Hofmann et al., 2010). We assumed that sidewelling irradiance illuminated fish, downwelling irradiance illuminated rock substrates, and the visual system was adapted to sidewelling irradiance for colour constancy. When computing Q_i for particular angular radiance, S was omitted and the radiance spectrum replaced I in Eqn 4. The results of Eqn 4 were used for each cone class (i) to calculate contrast between pairs of spectra, Δf_i:

$$\Delta f_i = \ln\left[\frac{Q_i(spec\ 1)}{Q_i(spec\ 2)}\right]. \quad (6)$$

Receptor noise for each cone class, w_i, was determined following Koshitaka et al. (2008), in which the L receptor is assumed to have a noise value of 0.05, as other studies have done (Cheney et al., 2009; Siddiqi et al., 2004; Vorobyev, 2003). The noise values for the other two cone classes are calculated using their relative abundance in the retinal mosaic:

$$w_i = 0.05\sqrt{\frac{n_L}{n_i}}. \quad (7)$$

Metriaclima zebra has a square cone mosaic (Dalton et al., 2014) in which the ratio of S:M:L cones is 1:2:2.

Discrimination between two colours (ΔS) was computed as:

$$\Delta S = \sqrt{\frac{w_S^2(\Delta f_L - \Delta f_M)^2 + w_M^2(\Delta f_L - \Delta f_S)^2 + w_L^2(\Delta f_S - \Delta f_M)^2}{(w_S w_M)^2 + (w_S w_L)^2 + (w_M w_L)^2}}. \quad (8)$$

The ΔS units are just noticeable differences (JND), the smallest difference between two colours that can be discriminated by the visual system. To test for the effects of opsin coexpression (see Results) and simplify the modelling of colour discrimination, we calculated JNDs for pure visual pigments and compared it with four common coexpression combinations found in four retinal areas. These include: (1) coexpression in S-cones in the dorsal-temporal quadrant (50% *SWS2B*/0% *RH2Abeta*/0% *LWS*); (2) coexpression in S- and M-cones in the dorsal-nasal quadrant (50% *SWS2B*/50% *RH2Abeta*/0% *LWS*); (3) coexpression of S- and L-cones in the ventral-temporal quadrant (50% *SWS2B*/0% *RH2Abeta*/30% *LWS*); and (4) coexpression of all three cone types in the ventral-nasal quadrant (50% *SWS2B*/50% *RH2Abeta*/30% *LWS*).

Achromatic contrast detection was examined by modelling the greatest distance at which a black object could be detected by single cones when viewed horizontally or directly overhead against the corresponding spacelight background. Calculations were performed according to Dalton et al. (2014) following the methods of Lythgoe (1968). The Weber contrast, C_r, of a dark object viewed horizontally against a bright background is calculated from:

$$C_r = \frac{\int_{300}^{700} N_{Tr}(\lambda)p_V(\lambda)T(\lambda)d\lambda - \int_{300}^{700} N_B(\lambda)p_V(\lambda)T(\lambda)d\lambda}{\int_{300}^{700} N_B(\lambda)p_V(\lambda)T(\lambda)d\lambda}, \quad (9)$$

where N_{Tr} is target radiance at viewing distance r, p_V is visual pigment absorptance, T is lens transmittance and N_B is radiance of the water background (horizontal spacelight), which we measured directly and is independent of r. The target radiance is altered by attenuation and by intervening light scattered into the visual path. It is quantified as:

$$N_{Tr} = \int_{300}^{700} N_{T0}e^{-ar}d\lambda + \int_{300}^{700} N_B(1 - e^{-ar})d\lambda, \quad (10)$$

where N_{T0} is the target radiance when r=0, and a is the beam attenuation coefficient. For a black object, the target radiance, and hence the first term, is taken to be zero. The second term of this equation corresponds to intervening light. For objects viewed horizontally, the amount and spectrum of light that enters the horizontal visual path between object and viewer is considered to be the same at all points along the visual path. However, this does not hold for objects viewed overhead. In this case, we estimated intervening light scattered into the visual path at a given viewing depth (r) by subtracting the beam attenuated radiance (L_b) from the diffuse attenuated radiance (L_d). These can be determined from the radiance just below the water's surface, L_0, the diffuse attenuation coefficient, A (Sabbah et al., 2011), and the beam attenuation coefficient, a (Dalton et al., 2010; Table S1E):

$$N_{Tr,black} = \int (L_d - L_b)d\lambda = \int [L_0(1 - e^{-Ar}) - L_0(1 - e^{-ar})]d\lambda\,. \quad (11)$$

Achromatic contrast and the distance at which contrast was at threshold (0.02) were compared for single cones expressing pure *SWS1* or a mixture with 50% *SWS2B*. We also compared individual double cones with 0 or 50% *RH2Abeta* mixed with *RH2B* and 0 or 30% *LWS* mixed with *RH2Aalpha*. Finally, we considered the sum of both double cones or the sum of all three cones acting as a single luminance channel. We assumed the horizontally viewed object was located 3 m below the water surface and the overhead object was just below the surface.

RESULTS

Topographic distribution of ganglion cells and spatial resolving power

The density and topographic distribution of ganglion cells was assessed in three different individuals of *M. zebra*. Overall, the data obtained were very similar between the three individuals, with a

Table 1. Summary of the ganglion cell data obtained using the optical fractionator method for three individuals of *Metriaclima zebra*

Individual	Standard length (mm)	Total number	Peak density (cells mm^{-2})	CE	Lens ø (mm)	SRP (cycles deg^{-1})
Mz 124	99	470,453	16,200	0.033	3.00	4.34
Mz 126	102	430,316	15,600	0.036	3.18	4.51
Mz 127	96	467,369	17,200	0.037	3.20	4.76

CE, Schaeffer coefficient of error; Ø, diameter; SRP, spatial resolving power.

Journal of Experimental Biology (2017) 220, 266-277 doi:10.1242/jeb.149211

mean total number of cells of 456,046 and mean peak density of 16,333 cells mm^{-2} (Table 1).

The topographic pattern of ganglion cell distributions revealed two retinal specializations (Fig. 2A, Fig. S1): an area centralis and a weak horizontal streak. The area centralis is located in the temporal part of the retina close to the optic nerve head, with a peak cell density ranging from 15,600 to 17,200 cells mm^{-2} (Table 1). The iso-density lines in the area centralis are concentric and range from the peak density to approximately 9000 cells mm^{-2}. In the midperipheral retina, the iso-density lines become more elliptical and elongated, forming a weak horizontal streak with cell densities ranging from 6000 to 8000 cells mm^{-2}.

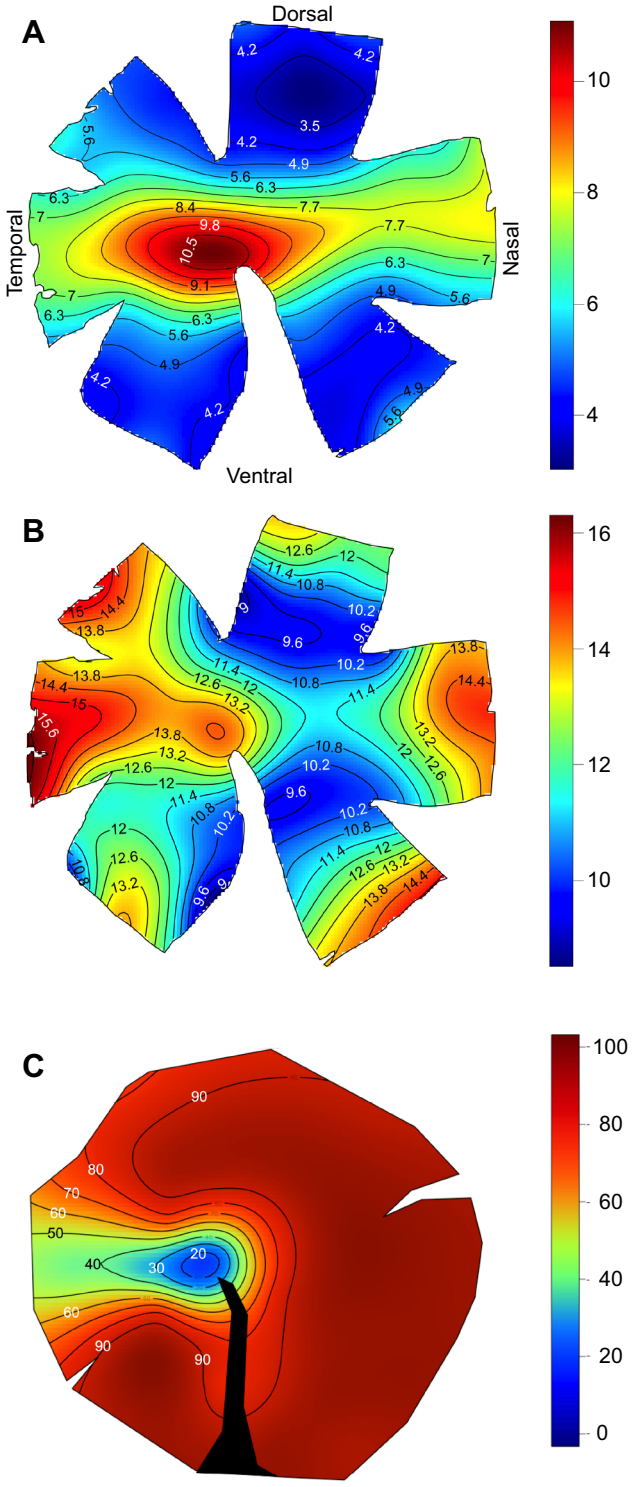

Fig. 2. Topographic distribution of ganglion cell densities, cone cell densities and opsin coexpression levels, in the same individual. (A) Density of retinal ganglion cells. (B) Density of all cone cells (single cones+double cones). (C) Percent of single cones coexpressing *SWS2B* with *SWS1*. Colour bars: (A,B) thousands of cells per mm^2, (C) % of single cones coexpressing opsins. All retinas oriented as in A; right eye used for A and B, left eye for C. Black area in C indicates location of optic nerve head and falciform process.

Based on the peak ganglion cell densities, the SRP in *M. zebra* is 4.5 cycles deg^{-1} averaged across the three individuals (Table 1). We can use the SRP values to determine how far away cichlids can potentially resolve particular objects or patterns. *Metriaclima zebra* has a barred male colour pattern with bars that are 3–4 mm wide. For an SRP of 4.5 cycles deg^{-1}, where one cycle (one bright blue bar and one black bar) is approximately 7 mm wide, this pattern could be resolved at a distance of 1.8 m or less. This distance is consistent with distances at which females choose whether to engage courting males and males choose whether to defend their territory against neighbouring males (1–2 m; K.C., personal observation). Visual acuity is also key for capturing prey items, with some of the smallest being zooplankton. Zooplankton of Lake Malawi vary in size from 200 to over 1000 µm (Irvine and Waya, 1999). Similar acuity calculations can be used to determine that *M. zebra* can resolve a zooplankter from its background at distances of 10 to 50 cm. This distance seems reasonable, as cichlids have been observed moving over relatively short distances (2–5 cm; K.C., personal observation) as they search for and pluck prey from the water column. Therefore, the SRP seems adequate to perform several key cichlid visual tasks.

Topographic distribution of cone photoreceptors

The density and topographic distribution of cone photoreceptors were assessed in three individuals of *M. zebra*. In two of these retinas (Mz 124 and Mz 126) we mapped both photoreceptors and ganglion cells (e.g. Fig. 2A,B). *Metriaclima zebra* had cones arranged in a regular fashion forming a mosaic composed of single cones, each surrounded by four double cones with a double to single cone ratio of 2:1. This mosaic pattern was consistent over the entire retina, resulting in similar topographic distributions for each cell type (Fig. S2). As a result, we will only describe in detail the distribution pattern for total cones.

The topographic distribution of cones was similar between individuals, though cell density did vary, with Mz 124 possessing higher densities than the other two individuals (Fig. S2). This slightly higher density for Mz 124 most likely reflects the somewhat smaller size of this particular individual. As the eye grows in larger teleost individuals, some cells are added in the retinal margin. However, overall, the existing retina is stretched, resulting in a decrease in absolute cell densities, and constant visual capabilities (Fernald, 1985). The average number of cones was 780,906 (Table 2). In contrast to ganglion cells, the highest cone densities were found in the nasal and temporal periphery. In addition, there was a general increase in cell density towards the periphery resulting from the presence of smaller cells. This was most marked for individual Mz 124 (Fig. 2) but occurred to a lesser degree for the other two individuals (Fig. S2). The peak density was between 17,800 and 19,400 cells mm^{-2} (Table 2). However, cone densities were similar to the ganglion cell pattern in having an area centralis in the temporal part of the retina close to the optic nerve head, with a peak cone cell density ranging from 12,000 to 14,000 cells mm^{-2} (Fig. S2). A weak horizontal streak, analogous to the one formed by the ganglion cells, could also be identified, although it was slightly obscured by the increase in cell density present toward the periphery.

Journal of Experimental Biology (2017) 220, 266-277 doi:10.1242/jeb.149211

Table 2. Summary of the photoreceptor cell quantitative data obtained using the optical fractionator method for three individuals of *M. zebra*

Indiv	Total DC	Peak DC (cells mm^{-2})	Total SC	Peak SC (cells mm^{-2})	Total cones	Peak TC (cells mm^{-2})	CE
Mz 124	520,266	13,300	248,979	6100	769,245	19,400	0.036
Mz 125	530,744	12,900	256,626	5600	787,371	18,200	0.027
Mz 126	530,955	12,600	248,979	5300	786,103	17,800	0.030

Standard length for Mz 125 was 112 mm, lengths for others given in Table 1. DC, double cones; SC, single cones; TC, total cones; CE, Schaeffer coefficient of error.

Coexpression of opsins in single cones and double cones

Single cones

Using fluorescent *in situ* hybridization of whole retinas, we found *SWS1* and *SWS2B* were expressed in single cones but never in double cones (Fig. 3). *SWS1* was essentially always expressed in single cones (99.8±0.2% of all the single cones examined in five of the six individuals; single cone n=8150). However, one individual (I6) had one region of the retina where *SWS2B* expression predominated (dorso-nasal margin, where 81.0% of single cones expressed only *SWS2B*; n=200 cells). This individual still had high *SWS1* expression in singles cones overall (90.7%; n=1900).

In contrast to *SWS1*, the level of *SW2B* expression varied considerably among individuals, from 20.7 to 95.6%. Although it varied in extent, the spatial distribution of *SWS2B* was consistent across the retinas of all individuals (Fig. 4). *SWS2B* was most likely to be expressed in the nasal retina and less likely in a region that was located slightly temporally from the center of the retina, extending temporally and dorsally (Fig. 4). Therefore, the area centralis region had less coexpression than other parts of the retina. The extensive individual variation in single cone coexpression is similar to what we found previously for opsin coexpression variation in double cones (Dalton et al., 2014).

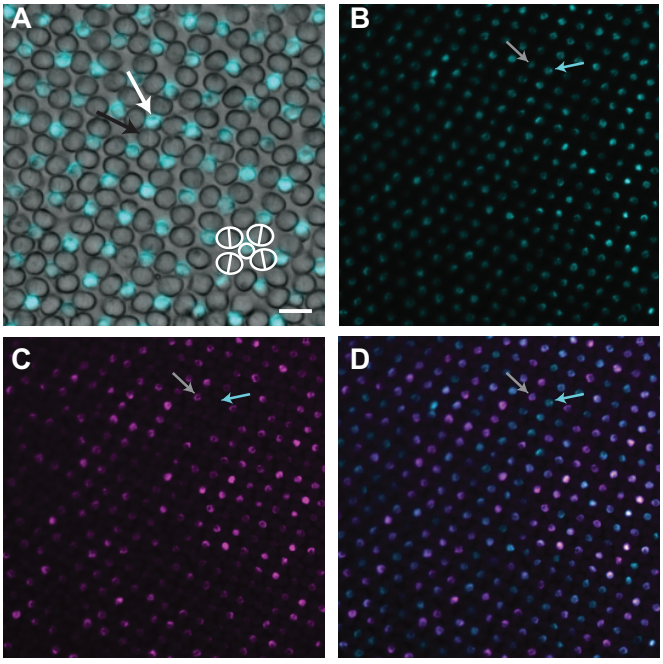

Fig. 3. *SWS1* and *SWS2B* are coexpressed in single cones. (A) *In situ* hybridization shows *SWS1* (cyan) is expressed in single cones but not in double cones. (B,C) Nearly all single cones express *SWS1* (B, cyan). Single cones may also express *SWS2B* (C, violet, and merged image D). Grey arrow indicates a coexpressing single cone (B–D). Some single cones (cyan arrow) express *SWS1* only. Scale bar: 25 µm.

Double cones

We showed previously that *RH2B* and *RH2Aalpha* are expressed in opposite members of nearly every double cone across the retina (Dalton et al., 2014). Combining this with the single cone results, we find that each unit of the retinal mosaic has *SWS1* in the central single cone and *RH2B* and *RH2Aalpha* in opposite members of each double cone. Previously, we also found spatially varying coexpression in double cones (Dalton et al., 2014). In the nasal retina *RH2Abeta* is often coexpressed with *RH2B*, but this becomes less common toward the middle retina and is rare in temporal regions. The *RH2Aalpha* members coexpress *LWS* frequently in the ventral retina but rarely in the dorsal retina. Thus coexpression in double cones is low in the dorsotemporal retina. To further characterize this infrequent dorsotemporal coexpression, we re-examined previously fixed retinal samples from two fish shown to have unusually high coexpression in the more dorsal and temporal regions (Dalton et al., 2014, 2015). This extended the five regions transected previously to more globally sample opsin expression across the entire retina, similarly to what we did for the single cones in the present study. For coexpression of *LWS* with *RH2Aalpha*, the expansion of LWS coexpression into the dorsal hemisphere was limited to the mid and nasal retina and did not occur in the temporal retina (Fig. 5A). Likewise, for coexpression of *RH2Abeta* with *RH2B*, the extension of *RH2Abeta* coexpression into the temporal hemisphere was greater in the ventral than in the dorsal retina (Fig. 5B). Thus, there is minimal opsin coexpression in both single and double cones in the dorsotemporal retina, including the area centralis.

Effects of opsin coexpression on visual function

Colour discrimination

To examine the possible effects of coexpression on colour vision, we modelled the ability of *M. zebra* to discriminate *M. zebra* colours from different viewing backgrounds as well as to discriminate between foraging rock substrates. This compared the visual system typical of the area centralis based on pure *SWS1*, *RH2B* and *RH2Aalpha* visual pigments (no coexpression: 0% *SWS2B*/0% *RH2Abeta*/0% *LWS* in S/M/L cones) with four common coexpression combinations found in the four retinal quadrants. When colour discrimination is calculated for pure visual pigments without any coexpression, most colour comparisons are above 5 JNDs (Table S2A). Coexpression decreased JNDs of most colour–background comparisons quite significantly, though JNDs of other colour comparisons showed slight increases (Fig. 6, Table S2A). These changes are only important if JNDs are close to threshold (less than 5), and so we have greyed out JNDs that are above this value (Kemp et al., 2015). This still leaves many of the fish colours when viewed against the spacelight or rocks less well discriminated as a result of coexpression. The only exceptions where coexpression did not hinder discrimination of colour combinations were for horizontal viewing against two broader spacelight spectra (Thumbi West Island and Otter Point) and a few of the rock backgrounds (Table S2A). Coexpression in single cones (adding SWS2B to SWS1) caused a substantial decrease in JNDs in comparisons

Journal of Experimental Biology (2017) 220, 266-277 doi:10.1242/jeb.149211

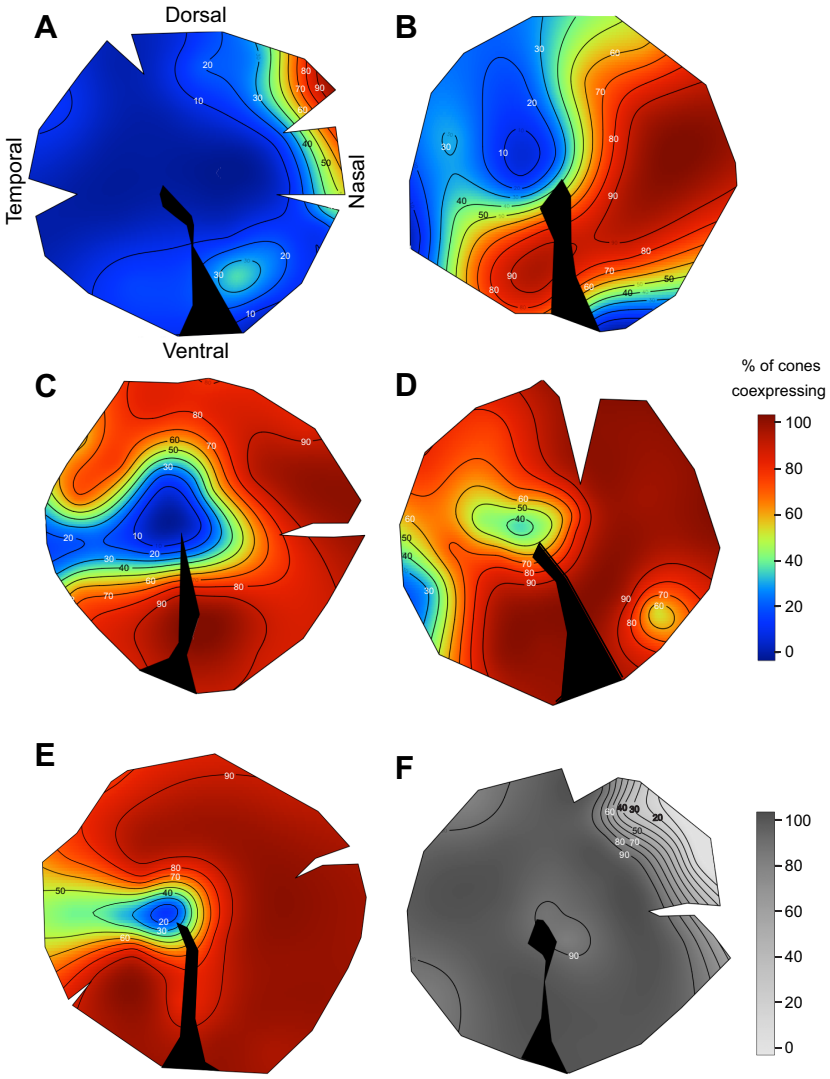

Fig. 4. Frequency of opsin coexpression in single cones across the retina of *Metriaclima zebra* in six individuals. (A–E) Percent coexpressing *SWS2B* with *SWS1*. Non-coexpressing single cones expressed *SWS1* only. (F) Percent coexpressing *SWS1* with *SWS2B*. Non-coexpressing single cones expressed *SWS2B* only (greyscale).

between rock substrates, regardless of the degree of coexpression in the double cone cells (Fig. 6, Table S2A). This suggests that coexpression would hinder algal foraging among the aufwuchs by reducing colour discrimination between different aufwuchs-covered rock surfaces.

We also considered colour discrimination among different cichlid colours (Table S2B). Surprisingly, when coexpression had an effect, more than half of those within cichlid colour comparisons benefited from coexpression, increasing their JND. Although many of these improvements occurred for comparisons well above the JND

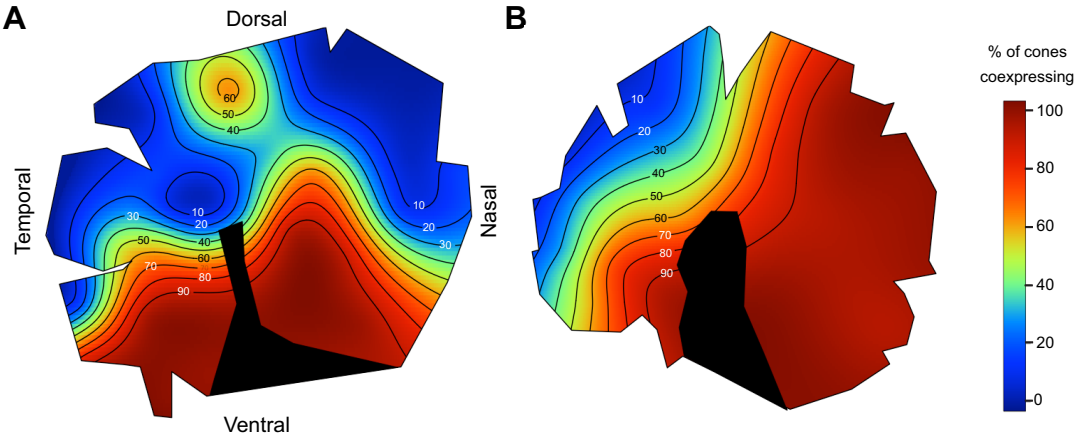

Fig. 5. Frequency of opsin coexpression in double cones across the retina of *M. zebra* in two individuals previously sampled at only five retinal locations. (A) Percent coexpression of *LWS* with *RH2Aalpha* (reanalyzed from Dalton et al., 2015) and (B) percent coexpression of *RH2Abeta* with *RH2B* (reanalyzed from Dalton et al., 2014).

Journal of Experimental Biology (2017) 220, 266-277 doi:10.1242/jeb.149211

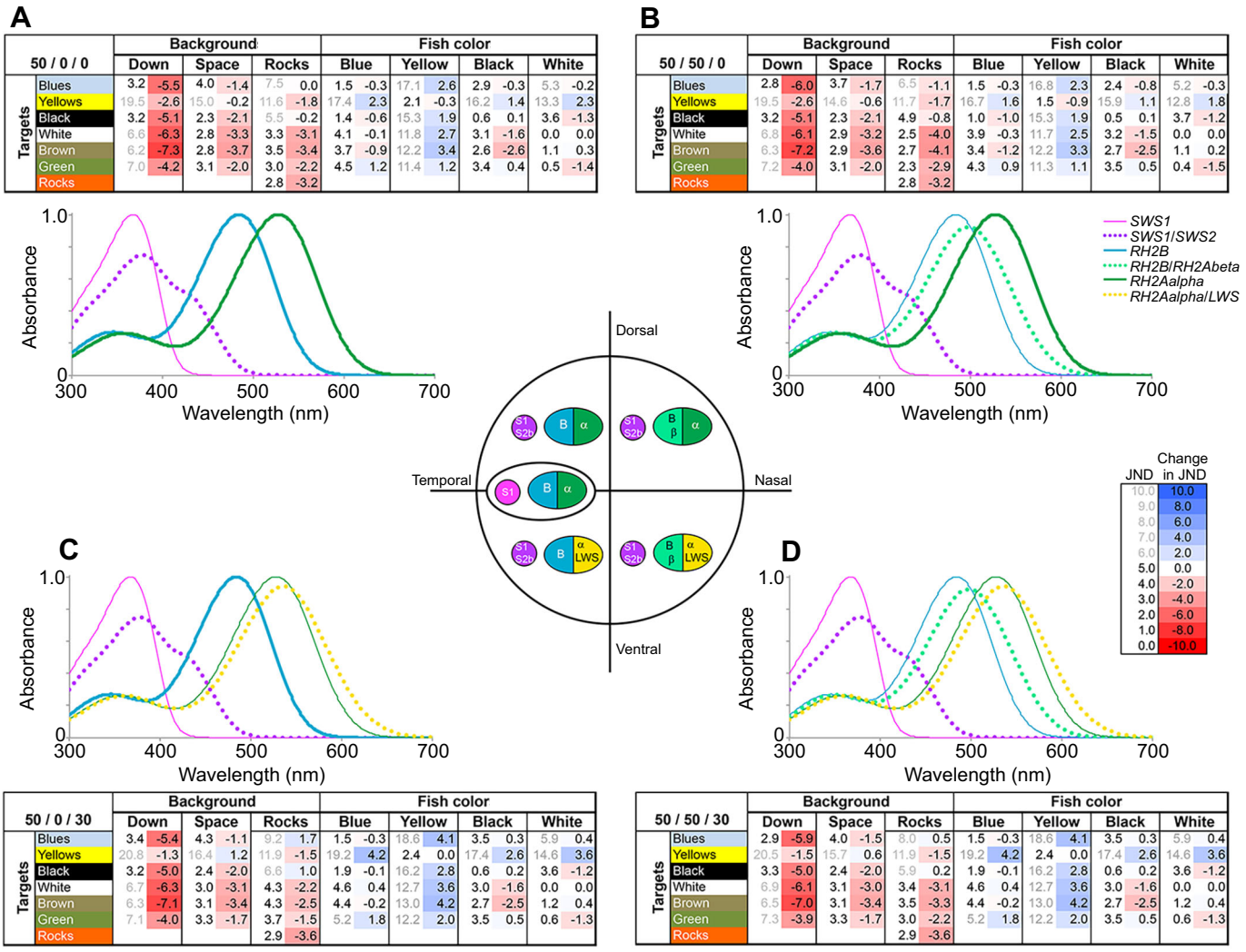

Fig. 6. Effects of opsin coexpression on colour discrimination [just noticeable differences (JNDs)]. The targets are either cichlid colours (illuminated by sidewelling irradiance) or rocks (illuminated by downwelling irradiance). JNDs are calculated for the target spectra compared with either different backgrounds [downwelling radiance (down), sidewelling radiance (space), or rocks] or other cichlid colours (blue, yellow, black, white). Comparisons are averages of several targets and several background measurements (for individual targets and backgrounds, see Table S2A,B). For each comparison, the JND is given (first column) as well as the change in JND relative to the JND for pure visual pigments (second column coloured as heat map, with blue being a JND increase and red a decrease with coexpression). Pure pigments are shown in the area centralis and include *SWS1* (S1) expressed in short single (S) cones and *RH2B* (B) and *RH2Aalpha* (α) expressed in medium (M) and long (L) double cones. We compare pure pigments to four different coexpression combinations, where we note the percent coexpression in S-, M- and L-cones. The four quadrants have the following visual pigment combinations: (A) coexpressing S-cones with 50/50 mix of *SWS1*/*SWS2B* (S1/S2b): 50/0/0; (B) coexpressing S- and M-cones with 50/50 mix of both *SWS1*/*SWS2B* and of *RH2B*/*RH2Abeta* (B/β): 50/50/0; (C) coexpressing S- and L-cones with 50/50 mix of *SWS1*/*SWS2B* and 70/30 mix of *RH2Aalpha*/*LWS* (α/LWS): 50/0/30; and (D) coexpression in all three cone types: 50/50/30. Also shown are absorbance spectra of the corresponding visual pigments found in each quadrant. The thin lines are the pure pigments. The actual visual pigment combinations are shown as a dotted line if coexpressed or a thicker solid line if a pure pigment. The central figure summarizes the coexpression combinations considered in the four quadrants in comparison to the temporal area centralis region containing pure pigments. Single cones are shown as one circle and double cones are shown as the joined half ovals. Genes expressed in these cones are listed with cones colour-coded to correspond to the visual pigment spectra.

threshold, this still suggests that coexpression does not always decrease colour discrimination. This is likely a result of colours that are well separated (blue versus yellow) benefiting from an increase in coexpression. These are common cichlid colour combinations, suggesting that coexpression might help with discriminating bars or egg spots from their surrounding colours (Dalton et al., 2010).

Achromatic contrast detection

Coexpression of *SWS1*/*SWS2B* greatly increased absorbance of spacelight and extended detection distances for contrast detection of dark objects. A 50:50 mixture of *SWS1*:*SWS2B* absorbs 133 to 177% more of all background radiances, as measured every 15 deg from zenith to nadir (see Dalton et al., 2014). The increase in absorption was 166% for overhead radiance (downwelling) and 162% for horizontal spacelight. Coexpression increased contrast of a dark object viewed horizontally at all distances modelled; however, the largest absolute gains in contrast occurred at shorter viewing distances (Table 3). The detection distances at which single cones were able to distinguish a dark object from the bright background illumination were also substantially increased by pigment mixtures. Compared with pure *SWS1*, a 50:50 mix of *SWS1*/*SWS2B* increased the detection distance of a horizontally viewed dark object by 24.5%

Journal of Experimental Biology (2017) 220, 266-277 doi:10.1242/jeb.149211

Table 3. Contrast detection comparing pure pigments and coexpressing pigments for detecting a dark object against the sidewelling spacelight

Contributing cone	Pigment	Distance (m)	Contrast	Contrast improvement (%)	Distance improvement (%)
S	*SWS1*	8.68	0.02		
	50/50 *SWS1*/*SWS2B*	8.68	0.042	110	
		10.81	0.02		24.5
M*	*RH2B*	12.95	0.02		
	50/50 *RH2B*/*RH2Abeta*	12.95	0.0217	8.6	
		13.23	0.02		2.1
L*	*RH2Aalpha*	13.585	0.02		
	70/30 *RH2Aalpha*/*LWS*	13.585	0.0205	1.2	
		13.63	0.02		0.45
M+L	*RH2B*+*RH2Aalpha*	13.29	0.02		
	50/50 *RH2B*/*RH2Abeta*+70/30 *RH2Aalpha*/*LWS*	13.29	0.0208	4.2	
		13.43	0.02		1.0
S+M+L	*SWS1*+*RH2B*+*RH2Aalpha*	13.13	0.02		
	50/50 *SWS1*/*SWS2B*+50/50 *RH2B*/*RH2Abeta*	13.13	0.02018	0.9	
	70/30 *RH2Aalpha*/*LWS*	13.15	0.02		0.15

Contrast improvement is the increase in contrast of the mixed pigment at the distance at which the pure pigment reaches detection threshold, compared with the pure pigment contrast (2%). Distance improvement is the increase in the detection distance of the mixed pigments (at 2% contract) relative to the pure pigment(s).
*Data for M and L cones similar to results in Dalton et al., 2014.

(from 8.68 to 10.81 m; Table 3). For a dark object viewed overhead, the detection distance increased from 17.0 m (for pure *SWS1*) to 18.35 m (7.9% increase; Table 4). When the signals of S-cones are summed with those of M- and L-cones, the improvement of S-cone coexpression on horizontal detection distance only increases by 0.15%. However, it is unknown whether the S channel is processed independently or summed with the M and L channels. We previously showed that coexpression in M and L cones improves contrasts (1–8.5%) and detection distances (0.5–2%) (Dalton et al., 2014), and those results are again included in Tables 3 and 4.

DISCUSSION

Cichlids have sufficient visual acuity

We have shown that *M. zebra* has an area centralis with maximal ganglion cell density and high cone cell density located in the temporal retina near the optic nerve head (Fig. 2). The area centralis has higher visual acuity and is likely important for looking forward for object recognition and discrimination. The estimated SRP of 4.5 cycles deg^{-1} in a Lake Malawi cichlid is similar to values obtained from Lake Victorian cichlids (SRP=3.3 to 3.9 cycles deg^{-1}; van der Meer and Bowmaker, 1995). These data suggest that cichlid visual acuities are poorer than those observed for some coral reef fish [*Choerodon albigena* (SRP=15 cycles deg^{-1}) or *Gymonocranius bitorquotus* (SRP=27 cycles deg^{-1})] but similar to others [*Dasson variabilis* (SRP=4 cycles deg^{-1}) and *Amblyglyphidodon curacao* (SRP=7 cycles deg^{-1}); Collin and Pettigrew, 1989]. Although cichlids do not appear to have particularly high spatial resolution, our calculations indicate that the visual acuity of *M. zebra* is sufficient for key tasks involved in recognizing colour pattern elements for communication and discriminating prey items in foraging.

Opsin coexpression is highly variable

Individuals varied in the amount of single cone opsin coexpression. For one individual, there was very little coexpression. In four of the five retinas with significant coexpression, single cone coexpression followed a consistent pattern, being low in the area centralis and higher in the rest of the retina. The fifth individual showed high levels of coexpression across most of the retina (Fig. 4). Coexpression in double cones was also rare in the area centralis region, instead being concentrated in the nasal and ventral retina (Dalton et al., 2014). Thus coexpression in all cone types tends to be

Table 4. Contrast detection comparing pure pigments and coexpressing pigments for detecting a dark object against the downwelling radiance

Contributing cone	Pigment	Distance (m)	Contrast	Contrast improvement (%)	Distance improvement (%)
S	*SWS1*	17	0.02		
	50/50 *SWS1*/*SWS2B*	17	0.0267	33.3	7.9
		18.35	0.02		
M*	*RH2B*	17.22	0.02		
	50/50 *RH2B*/*RH2Abeta*	17.22	0.204	1.65	0.41
		17.29	0.02		
L*	*RH2Aalpha*	17.47	0.02		
	70/30 *RH2Aalpha*/*LWS*	17.47	0.0207	3.25	1.37
		17.71	0.02		
M+L	*RH2B*+*RH2Aalpha*	17.37	0.02		
	50/50 *RH2B*/*RH2Abeta*+70/30 *RH2Aalpha*/*LWS*	17.37	0.0205	2.27	0.58
		17.47	0.02		
S+M+L	*SWS1*+*RH2B*+*RH2Aalpha*	17.36	0.020		
	50/50 *SWS1*/*SWS2B*+*50*/*50 RH2B*/*RH2Abeta*+70/30 *RH2Aalpha*/*LWS*	17.36	0.0207	3.21	0.84
		17.505	0.020		

Contrast improvement is the increase in contrast of the mixed pigment at the distance at which the pure pigment reaches detection threshold, compared with that limiting pure pigment contrast (2%). Distance improvement is the increase in the detection distance of the mixed pigments relative to the pure pigment(s).
*Dalton et al., 2014.

Journal of Experimental Biology

Journal of Experimental Biology (2017) 220, 266-277 doi:10.1242/jeb.149211

lowest in the retinal region that is capable of the highest spatial resolution.

Coexpression variation may result from trade-offs between contrast detection and colour discrimination

Coexpression in particular regions and avoidance in others raises questions about specialization of retinal regions for different visual tasks and the role of coexpression in those specializations. Our modelling indicates that coexpression in all three cone classes could enhance achromatic contrast detection. Although these changes can be significant (>20%), in other cases those enhancements are only a few percent (Tables 3 and 4). While it is difficult to know what effects a 1–2% change in contrast or detection distance would be, such subtle changes could have large fitness effects if they enable females that are mouthbrooding their young to protect them from egg predators even a small fraction of the time. Such contrast advantages are offset by coexpression interfering with colour discrimination. Coexpression likely hinders colour discrimination between different foraging substrates and between at least some cichlid colour signals and viewing backgrounds. Thus, the area centralis has the highest acuity and consistently good colour vision owing to its low frequency of opsin coexpression.

In contrast to some of these results, we also find that increasing coexpression would actually increase the JNDs between some cichlid colours (Fig. 6, Table S2B). This may be because the reflectance spectra of some cichlid colours are spectrally broad and therefore better matched by broader visual pigments. Or it may be that coexpression spaces out the visual pigments to better match spectrally well-separated colours. However, these colour comparisons already have quite large JNDs well above the 5 JND threshold. Therefore, it may be that colour discrimination in the area centralis is already sufficiently large for female mate choice or male recognition of conspecific challengers. Further modeling is required to determine when and why these differences occur.

In addition to good colour vision, the area centralis may also have good contrast vision for certain targets. The area's high density of ganglion cells and S-cones exclusively expressing the UV-sensitive *SWS1* opsin may optimize detection of plankton that are transparent to longer wavelengths but less so to UV light. Ecological studies of cichlids add support to this hypothesis. *SWS1* expression in Lake Malawi cichlids is strongly correlated with zooplanktivory, as well as foraging on algae that grow on rocks (Carleton et al., 2016). The visual streak, which runs across the middle of the retina from nasal to temporal, also has relatively high acuity with higher coexpression towards the nasal margin, favouring contrast detection, and lower coexpression towards the temporal margin, favouring colour discrimination. In the nasal retina, both the increases in acuity and detection distance from coexpressing M-cones may contribute to enhanced detection of dark objects, such as predators, approaching from behind. The dorsal and ventral retinal margins have slightly elevated acuity (density) while maintaining a roughly 1:3 ratio of retinal ganglion cells to photoreceptors.

Combined with our previous work (Dalton et al., 2014), we have shown that *M. zebra* has three spectrally distinct classes of cone cells, one single cone (S-cone) and two double cone members (M- and L-cones). In addition to expressing one opsin in nearly every instance, each class also coexpresses the opsin that is its spectral neighbor and sensitive to longer wavelengths (Fig. 6). These opsins are not the genes that are nearest in the genome, ruling out a random sharing of promoters leading to random coexpression (O'Quin et al., 2011). Our results indicate that coexpressing single cones may enhance contrast detection of dark objects over a range of viewing distances less than 10.5 m (Fig. S3). It has not been demonstrated whether single cones contribute to achromatic tasks in cichlids. Another study showed that archerfish have single cones that match the background spectrum, suggesting they might be important for achromatic contrast detection (Temple et al., 2010).

Individual genetic variation as a possible cause for phenotypic variation

Our results suggest that selection for colour vision for cichlid colours against backgrounds would decrease coexpression while selective forces that favor achromatic contrast detection of dark objects would increase coexpression. We have recently shown that genetic control of certain cichlid opsins has a relatively simple genetic basis centred on variation of just a few key transcription factors (O'Quin et al., 2012; Schulte et al., 2014). If coexpression in a given cone class is controlled by two different alleles of a transcription factor, the opposing selective forces of colour discrimination versus contrast detection might result in a balanced polymorphism for that locus. Maintenance and alternative sorting of these alleles through the population would explain some of the variation in opsin expression observed between individuals in the wild and the laboratory. Those animals inheriting two alleles for low coexpression would have more cones expressing a single opsin, those with two alleles for high coexpression would have many coexpressing cones, and most of the heterozygous individuals would have an intermediate number of coexpressing cones.

This large predicted individual variation is indeed what we see. Although *SWS2B* expression was most common in the nasal retina and least common in the area centralis, we found significant variation in the spatial extent and overall level of *SWS2B* expression by different individuals. In the extreme individual (I6), *SWS2B* completely replaced *SWS1* in most of the cells in the nasal retina. In spite of the individual variation, coexpression in each cone class has a frequency gradient that follows a consistent spatial pattern across the retina.

It is worth noting that within regions where many cells are coexpressing, there are also many cells that express only one opsin. Thus coexpression shows patchiness on a fine scale. This is different from what has been reported in the mouse, where the relative amount of a coexpressed opsin changes across the retina, but in a given region the individual cells all have similar amounts of the two opsins (Applebury et al., 2000, 2007). Because variation in coexpression results in variation in λ_{max}, the patchiness of coexpression raises the possibility that there are more than three spectrally distinct cone types at different locations in the retina. Though it seems unlikely, this could lead to enhanced colour vision capabilities. Further experiments involving electrophysiology or behavior would be required to test for any increases in colour discrimination.

Conclusions

Regions of the cichlid retina differ in cell density and opsin expression. It is possible that these regions are specialized for different visual tasks. Individuals show consistent visual acuity, as determined by both photoreceptor and ganglion cell densities, that are well matched to finding food and finding mates. Opsin coexpression is reduced in the area centralis, where it could impede colour discrimination important for object recognition and high visual acuity tasks. Coexpression occurs frequently in both single and double cones in the retinal periphery, where it could enhance tasks involving contrast detection. One obvious alternative to the functional role of opsin coexpression is that it may have no

effect on visual tasks and just vary randomly between individuals. It might also have contrasting effects that are working against each other. Indeed, modelling indicated that coexpression is sometimes favourable for colour discrimination (comparisons between cichlid colours) and sometimes not (comparison of cichlid colours against backgrounds or rock substrates from each other). Further work is required to better understand how opsin coexpression is controlled as well as how the cichlid retina is wired for colour vision.

Acknowledgements
We thank two anonymous reviewers for their helpful comments and suggestions.

Competing interests
The authors declare no competing or financial interests.

Author contributions
B.E.D. performed *in situ* hybridization and visual modeling. F.d.B. performed the retinal whole mounts. K.L.C. and N.J.M. refined the visual modeling. All authors participated in the writing of the manuscript and approved its final form.

Funding
This work was supported by funding from the National Eye Institute of the National Institutes of Health [1R01EY024639 to K.L.C.] and the Australian Research Council (ARC) [to N.J.M.]. Stereology work was performed in the Queensland Brain Institute's Advanced Microscopy Facility and generously supported by ARC LIEF LE10010074.

Supplementary information
Supplementary information available online at
http://jeb.biologists.org/lookup/doi/10.1242/jeb.149211.supplemental

References

Allison, W. T., Barthel, L. K., Skebo, K. M., Takechi, M., Kawamura, S. and Raymond, P. A. (2010). Ontogeny of cone photoreceptor mosaics in zebrafish. *J. Comp. Neurol.* **518**, 4182-4195.

Applebury, M. L., Antoch, M. P., Baxter, L. C., Chun, L. L. Y., Falk, J. D., Farhangfar, F., Kage, K., Krzystolik, M. G., Lyass, L. A. and Robbins, J. T. (2000). The murine cone photoreceptor: a single cone type expresses both S and M opsins with retinal spatial patterning. *Neuron* **27**, 513-523.

Applebury, M. L., Farhangfar, F., Glösmann, M., Hashimoto, K., Kage, K., Robbins, J. T., Shibusawa, N., Wondisford, F. E. and Zhang, H. (2007). Transient expression of thyroid hormone nuclear receptor TRbeta2 sets S opsin patterning during cone photoreceptor genesis. *Dev. Dyn.* **236**, 1203-1212.

Baddeley, A. and Turner, R. (2005). spatstat: an R package for analyzing spatial point patterns. *J. Stat. Software* **12**, 1-42.

Baden, T., Schubert, T., Chang, L., Wei, T., Zaichuk, M., Wissinger, B. and Euler, T. (2013). A tale of two retinal domains: near-optimal sampling of achromatic contrasts in natural scenes through asymmetric photoreceptor distribution. *Neuron* **80**, 1206-1217.

Barthel, L. K. and Raymond, P. A. (2000). *In situ* hybridization studies of retinal neurons. *Methods Enzymol.* **316**, 579-590.

Briscoe, A. D., Bernard, G. D., Szeto, A. S., Nagy, L. M. and White, R. H. (2003). Not all butterfly eyes are created equal: rhodopsin absorption spectra, molecular identification, and localization of ultraviolet-, blue-, and green-sensitive rhodopsin-encoding mRNAs in the retina of *Vanessa cardui*. *J. Comp. Neurol.* **458**, 334-349.

Carleton, K. L., Dalton, B. E., Escobar-Camacho, D. and Nandamuri, S. P. (2016). Proximate and ultimate causes of variable visual sensitivities: insights from cichlid fish radiations. *Genesis* **54**, 299-325.

Cheney, K. L., Grutter, A. S., Blomberg, S. P. and Marshall, N. J. (2009). Blue and yellow signal cleaning behavior in coral reef fishes. *Curr. Biol.* **19**, 1283-1287.

Coimbra, J. P., Marceliano, M. L. V., Andrade-Da-Costa, B. L. S. and Yamada, E. S. (2006). The retina of tyrant flycatchers: topographic organization of neuronal density and size in the ganglion cell layer of the great kiskadee *Pitangus sulphuratus* and the rusty margined flycatcher *Myiozetetes cayanensis* (Aves: Tyrannidae). *Brain Behav. Evol.* **68**, 15-25.

Coimbra, J. P., Trévia, N., Videira Marceliano, M. L., Da Silveira Andrade-Da-Costa, B. L., Picanço-Diniz, C. W. and Yamada, E. S. (2009). Number and distribution of neurons in the retinal ganglion cell layer in relation to foraging behaviors of tyrant flycatchers. *J. Comp. Neurol.* **514**, 66-73.

Coimbra, J. P., Nolan, P. M., Collin, S. P. and Hart, N. S. (2012). Retinal ganglion cell topography and spatial resolving power in penguins. *Brain Behav. Evol.* **80**, 254-268.

Collin, S. P. and Collin, H. B. (1988). Topographic analysis of the retinal ganglion cell layer and optic nerve in the sandlance *Limnichthyes fasciatus* (Creeiidae, Perciformes). *J. Comp. Neurol.* **278**, 226-241.

Collin, S. P. and Pettigrew, J. D. (1989). Quantitative comparison of the limits on visual spatial resolution set by the ganglion cell layer in twelve species of reef teleosts. *Brain Behav. Evol.* **34**, 184-192.

Dalton, B. E., Cronin, T. W., Marshall, N. J. and Carleton, K. L. (2010). The fish eye view: are cichlids conspicuous? *J. Exp. Biol.* **213**, 2243-2255.

Dalton, B. E., Loew, E. R., Cronin, T. W. and Carleton, K. L. (2014). Spectral tuning by opsin coexpression in retinal regions that view different parts of the visual field. *Proc. R. Soc. B Biol. Sci.* **281**, 20141980.

Dalton, B. E., Lu, J., Leips, J., Cronin, T. W. and Carleton, K. L. (2015). Variable light environments induce plastic spectral tuning by regional opsin coexpression in the African cichlid fish, *Metriaclima zebra*. *Mol. Ecol.* **24**, 4193-4204.

de Busserolles, F., Fitzpatrick, J. L., Marshall, N. J. and Collin, S. P. (2014a). The influence of photoreceptor size and distribution on optical sensitivity in the eyes of lanternfishes (Myctophidae). *PLoS ONE* **9**, e99957.

de Busserolles, F., Marshall, N. J. and Collin, S. P. (2014b). Retinal ganglion cell distribution and spatial resolving power in deep-sea lanternfishes (Myctophidae). *Brain Behav. Evol.* **84**, 262-276.

Endler, J. A. (1993). Some general comments on the evolution and design of animal communication systems. *Philos. Trans. R. Soc. Lond. B Biol. Sci.* **340**, 215-225.

Escobar-Camacho, D. and Carleton, K. L. (2015). Sensory modalities in cichlid fish behavior. *Curr. Opin. Behav. Sci.* **6**, 115-124.

Fernald, R. D. (1985). Growth of the teleost eye: novel solutions to complex constraints. *Environ. Biol. Fish.* **13**, 113-123.

Garza-Gisholt, E., Hemmi, J. M., Hart, N. S. and Collin, S. P. (2014). A comparison of spatial analysis methods for the construction of topographic maps of retinal cell density. *PLoS ONE* **9**, e93485.

Glaser, E. M. and Wilson, P. D. (1998). The coefficient of error of optical fractionator population size estimates: a computer simulation comparing three estimators. *J. Microsc.* **192**, 163-171.

Govardovskii, V. I., Fyhrquist, N., Reuter, T., Kuzmin, D. G. and Donner, K. (2000). In search of the visual pigment template. *Vis. Neurosci.* **17**, 509-528.

Hofmann, C. M., O'Quin, K. E., Marshall, N. J., Cronin, T. W., Seehausen, O. and Carleton, K. L. (2009). The eyes have it: regulatory and structural changes both underlie cichlid visual pigment diversity. *PLoS Biol.* **7**, e1000266.

Hofmann, C. M., O'Quin, K. E., Marshall, N. J. and Carleton, K. L. (2010). The relationship between lens transmission and opsin gene expression in cichlids from Lake Malawi. *Vision Res.* **50**, 357-363.

Hughes, A. (1975). A quantitative analysis of the cat retinal ganglion cell topography. *J. Comp. Neurol.* **163**, 107-128.

Hughes, A. (1985). New perspectives in retinal organisation. *Prog. Retinal Res.* **4**, 243-313.

Irvine, K. and Waya, R. (1999). Spatial and temporal patterns of zooplankton standing biomass and production in Lake Malawi. *Hydrobiologia* **407**, 191-205.

Kelber, A., Vorobyev, M. and Osorio, D. (2003). Animal colour vision – behavioural tests and physiological concepts. *Biol. Rev. Camb. Philos. Soc.* **78**, 81-118.

Kemp, D. J., Herberstein, M. E., Fleishman, L. J., Endler, J. A., Bennett, A. T. D., Dyer, A. G., Hart, N. S., Marshall, J. and Whiting, M. J. (2015). An integrative framework for the appraisal of coloration in nature. *Am. Nat.* **185**, 705-724.

Koshitaka, H., Kinoshita, M., Vorobyev, M. and Arikawa, K. (2008). Tetrachromacy in a butterfly that has eight varieties of spectral receptors. *Proc. R. Soc. B Biol. Sci.* **275**, 947-954.

Land, M. F. and Nilsson, D.-E. (2001). *Animal Eyes*. Oxford: Oxford University Press.

Lythgoe, J. N. (1968). Visual pigments and visual range underwater. *Vision Res.* **8**, 997-1012.

Matthiessen, L. (1882). Ueber die beziehungen, welche zwischen dem brechungsindex des kerncentrums der krystalllinse und den dimensionen des auges bestehen. *Pflugers Arch.* **27**, 510-523.

Munz, F. W. and Mcfarland, W. N. (1977). Evolutionary adaptations of fishes to the photic environment. In *The Visual System in Vertebrates* (ed. F. Crescitelli), pp. 193-274. New York: Springer-Verlag.

O'Quin, K. E., Smith, D., Naseer, Z., Schulte, J., Engel, S. D., Loh, Y.-H. E., Streelman, J. T., Boore, J. L. and Carleton, K. L. (2011). Divergence in cis-regulatory sequences surrounding the opsin gene arrays of African cichlid fishes. *BMC Evol. Biol.* **11**, 120.

O'Quin, K. E., Schulte, J. E., Patel, Z., Kahn, N., Naseer, Z., Wang, H., Conte, M. A. and Carleton, K. L. (2012). Evolution of cichlid vision via trans-regulatory divergence. *BMC Evol. Biol.* **12**, 251.

Owens, G. L., Rennison, D. J., Allison, W. T. and Taylor, J. S. (2012). In the four-eyed fish (*Anableps anableps*), the regions of the retina exposed to aquatic and aerial light do not express the same set of opsin genes. *Biol. Lett.* **8**, 86-89.

Parry, J. W. L., Carleton, K. L., Spady, T., Carboo, A., Hunt, D. M. and Bowmaker, J. K. (2005). Mix and match color vision: tuning spectral sensitivity by

differential opsin gene expression in Lake Malawi cichlids. *Curr. Biol.* **15**, 1734-1739.

Sabbah, S., Gray, S. M., Boss, E. S., Fraser, J. M., Zatha, R. and Hawryshyn, C. W. (2011). The underwater photic environment of Cape Maclear, Lake Malawi: comparison between rock- and sand-bottom habitats and implications for cichlid fish vision. *J. Exp. Biol.* **214**, 487-500.

Schulte, J. E., O'Brien, C. S., Conte, M. A., O'Quin, K. E. and Carleton, K. L. (2014). Interspecific variation in Rx1 expression controls opsin expression and causes visual system diversity in African Cichlid fishes. *Mol. Biol. Evol.* **31**, 2297-2308.

Siddiqi, A., Cronin, T. W., Loew, E. R., Vorobyev, M. and Summers, K. (2004). Interspecific and intraspecific views of color signals in the strawberry poison frog *Dendrobates pumilio*. *J. Exp. Biol.* **207**, 2471-2485.

Slomianka, L. and West, M. J. (2005). Estimators of the precision of stereological estimates: an example based on the CA1 pyramidal cell layer of rats. *Neuroscience* **136**, 757-767.

Smith, A. R., D'annunzio, L., Smith, A. E., Sharma, A., Hofmann, C. M., Marshall, N. J. and Carleton, K. L. (2011). Intraspecific cone opsin expression variation in the cichlids of Lake Malawi. *Mol. Ecol.* **20**, 299-310.

Stone, J., Rapaport, D. H., Williams, R. W. and Chalupa, L. (1981). Uniformity of cell distribution in the ganglion cell layer of prenatal cat retina: implications for mechanisms of retinal development. *Brain Res.* **2**, 231-242.

Temple, S. E. (2011). Why different regions of the retina have different spectral sensitivities: a review of mechanisms and functional significance of intraretinal variability in spectral sensitivity in vertebrates. *Vis. Neurosci.* **28**, 281-293.

Temple, S., Hart, N. S., Marshall, N. J. and Collin, S. P. (2010). A spitting image: specializations in archerfish eyes for vision at the interface between air and water. *Proc. R. Soc. B Biol. Sci.* **277**, 2607-2615.

Ullmann, J. F. P., Moore, B. A., Temple, S. E., Fernández-Juricic, E. and Collin, S. P. (2012). The retinal wholemount technique: a window to understanding the brain and behaviour. *Brain Behav. Evol.* **79**, 26-44.

Van Der Meer, H. J. and Bowmaker, J. K. (1995). Interspecific variation of photoreceptors in four co-existing haplochromine cichlid fishes. *Brain Behav. Evol.* **45**, 232-240.

Vorobyev, M. (2003). Coloured oil droplets enhance colour discrimination. *Proc. R. Soc. B Biol. Sci.* **270**, 1255-1261.

Vorobyev, M., Brandt, R., Peitsch, D., Laughlin, S. B. and Menzel, R. (2001). Colour thresholds and receptor noise: behaviour and physiology compared. *Vision Res.* **41**, 639-653.

Wertheim, J. O., Murrell, B., Smith, M. D., Kosakovsky Pond, S. L. and Scheffler, K. (2015). RELAX: detecting relaxed selection in a phylogenetic framework. *Mol. Biol. Evol.* **32**, 820-832.

West, R. A. (1991). Optical properties of aggregate particles whose outer diameter is comparable to the wavelength. *Appl. Opt.* **30**, 5316-5324.

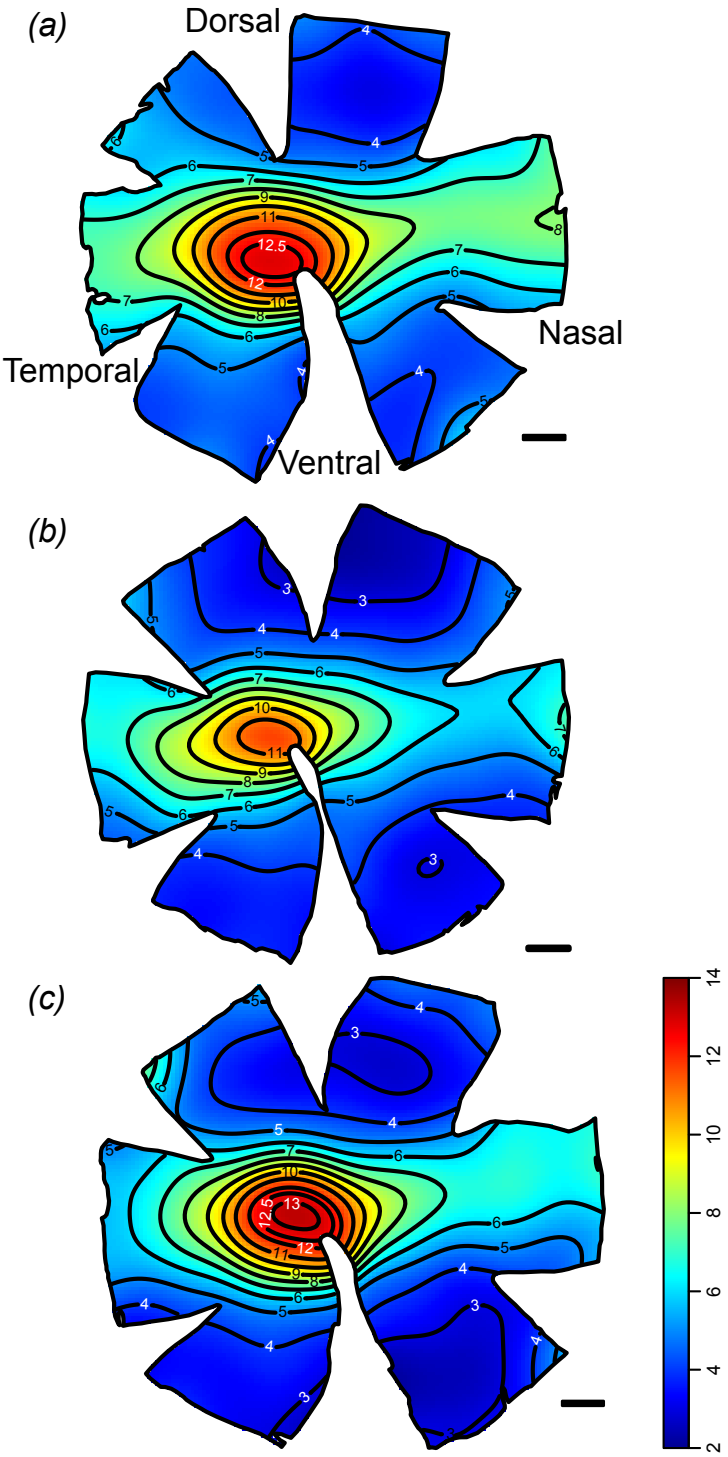

Supp. Fig. S1. Topographic distribution of retinal ganglion cell densities in three individuals. Ganglion cell density for individual in (a) also appear in Fig. 2. Density scales in thousands of cells per mm^2. Scale bars = 1 mm.

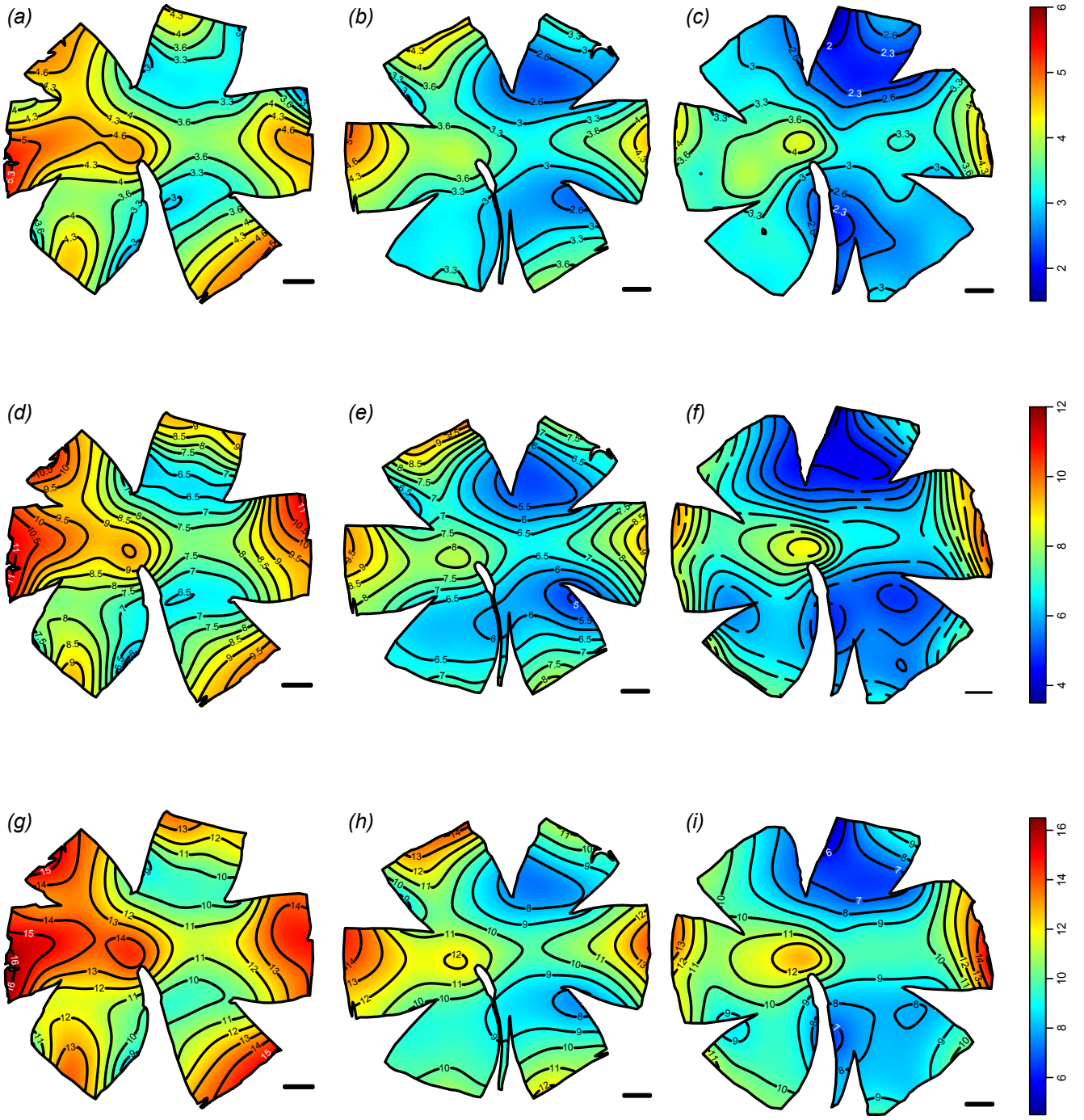

Supp. Fig. S2. Topographic distribution of single cones (a-c), double cones (d-f), and total cones (g-i) in three individuals. a, d, and g pertain to the individual from Fig. 2 (Mz 124); b, e, and h correspond to individual Mz 126; and c, f, and I correspond to individual Mz 127. Density scales in thousands of cells per mm^2. Scale bars = 1 mm.

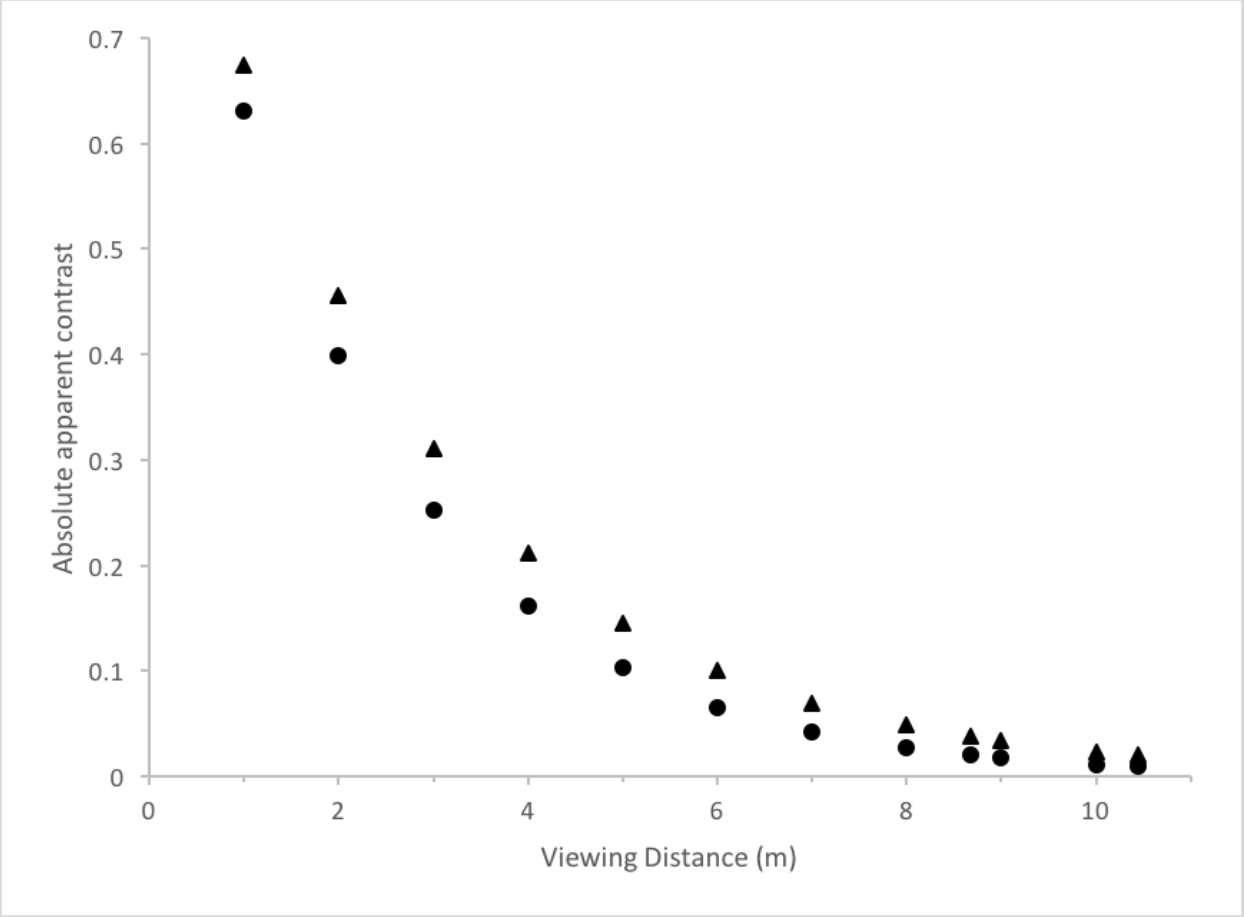

Supp. Fig. S3. Calculated apparent contrast of a dark object viewed horizontally against spacelight by S-cones expressing *SWS1* opsin only (circles) and by S-cones also coexpressing 30% *SWS2B* (triangles). Calculations used light spectra measured in Lake Malawi and assumed that viewer and object were 3 m below surface and that contrast threshold was 2%. Threshold was reached at viewing distance of 8.7 m for non-coexpressing S-cones and at 10.5 m for coexpressing S-cones.

Table S1

Click here to download Table S1

Table S2

Click here to download Table S2